Improving Terrain Navigation by Concurrent Tidal and Sound Speed Error Estimation

Ove Kent Hagen and Kjetil Bergh Ånonsen
Norwegian Defence Research Establishment (FFI)
P O Box 25, NO-2027 Kjeller, Norway
Email: ove-kent.hagen@ffi.no

***Abstract*—Terrain navigation in the presence of an unknown tide level has been demonstrated earlier, where both horizontal position and depth errors of a nominal navigation solution can be estimated concurrently. Accurate bathymetric measurements based on acoustic sensors also rely on knowing the sound speed near the sensor and in the water column between the sensor and the sea floor. This is important for vessels operating far from the sea floor, but also for underwater vehicles operating near the sea floor with side-looking bathymetric systems. To enable high performance terrain navigation in those scenarios, the sound speed error must also be considered. This paper proposes three different modifications to a 2D point mass filter to enable concurrent compensation for tide and sound speed error. Simulations so far indicate a great improvement compared to using a regular 2D point mass filter.**

I. Introduction

Terrain navigation is a technique increasingly used for subsurface position updates of Autonomous Underwater Vehicles (AUVs). By comparing bathymetric measurements with a digital terrain model (DTM), the best matching position may be used to update an aided inertial navigation system (INS). This efficiently bounds the position error of the AUV in suitable terrain, and several real-time systems have been developed to demonstrate the concept [1]–[4]. The technique has also been proposed and demonstrated as a technique for making surface vessels robust against GPS jamming- and spoofing attacks [5]. Common to both these scenarios is the use of acoustic sensors to measure the bathymetry. Accurate bathymetric measurements with acoustic sensors rely on knowing the sound speed through the water column between the sensor and the sea floor. Error in sound speed, both near the sensor and in the water column, together with inaccuracies in the ray propagation algorithm, results in errors, both in the estimated depth and in the location of the footprint on the sea floor. Usually a surface vessel is more susceptible to these errors, but there are cases for AUVs, even at low altitude, when sound speed errors are important [6]. This is especially true when using side-looking sonars with grazing angles, at which refraction of the acoustic signal increases. Another common error is due to the difference in the vertical datum of the DTM and the real-time bathymetric measurements. The DTM may be compensated for the tide level in post-processing, but in real-time the AUV and the surface vessel usually only know the predicted tide level, or simply refer the measured depth to current sea level. Fig. 1 gives an example of what is likely a combination of sound speed and tidal error when comparing real-time EM710 multibeam echo sounder measurements at the true position of the surface vessel H.U. Sverdrup II with a DTM constructed from post-processing an earlier survey with an EM1002 multibeam echo sounder [5]. Most of the bias in the profile is caused by the unknown tide level, but a smaller part of the bias and the curvature of the profile is most likely caused by a sound speed error.

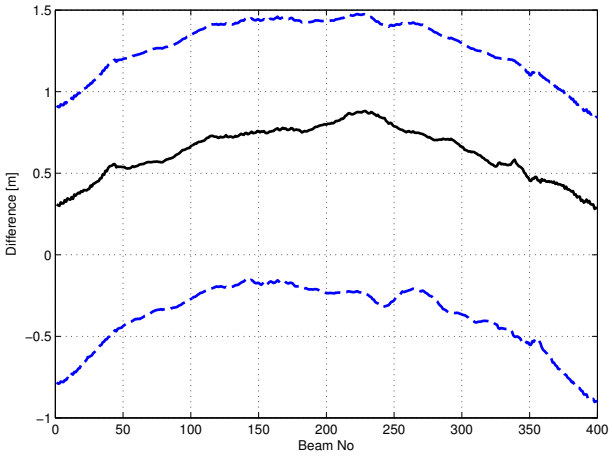

Fig. 1. Mean profile difference between 2.5 minutes of EM710 real-time measurements and a DTM based on post-processed EM1002 measurements (black) as a function of beam number, along with the standard deviation (broken blue).

In the most suitable terrain types, the terrain navigation algorithms converge even in the presence of this type of error, but in more suitable terrain the error may influence the convergence of the algorithms. This paper explores the idea of using the information in the difference profiles, as shown in Fig. 1, to concurrently estimate and compensate for the sound speed and tidal errors. Three approaches to integration of the sound speed and tidal error bias estimates with the point mass filter (PMF) terrain navigation algorithm are considered:

- Correct the measurements with the most likely bias estimates based on the last good position fix.
- Use an improved covariance model in the PMF estimator.
- Use a Rao-Blackwellized version of the PMF estimator.

The three new methods are compared to the relative profile method [7], amongst others used in the PMF implemented in

the HUGIN AUV terrain navigation system today [4]. Section II reviews the Bayesian formulation of terrain navigation, and the point mass filter estimator. An error model for the sound speed and tidal errors is developed, and three modified versions of the PMF are introduced. Simulations from two scenarios are used to test and compare the modified versions in Section III. Finally some preliminary conclusions and suggestions for future work are given in Section IV.

II. Terrain Navigation

A. Dynamic model

To enable practical calculation for the nonlinear terrain navigation problem, a simplified mathematical model for the dynamics of the surface vessel and the measurements of the bathymetric sensors is presented. Let $\boldsymbol{x}_k = (x_k, y_k, z_k)$ denote the vessel's position in a local north-east-down system at time $t = t_k$. Consider the following dynamical model for the position states of the vessel

$$\boldsymbol{x}_{k+1} = \boldsymbol{x}_k + \boldsymbol{u}_k + \boldsymbol{v}_k, \tag{1}$$

where $\boldsymbol{u}_k$ is the integrated motion estimated by the INS in the time interval t_k to t_{k+1}, and $\boldsymbol{v}_k$ is a white stochastic process modeling the error drift in the INS estimate.

B. Measurement model

Let $(\boldsymbol{\xi}_k^N, \boldsymbol{\eta}_k^N, \boldsymbol{\zeta}_k)$ denote m_k bathymetric depth measurements relative to the INS solution in a local level north aligned system N, and let $h(\boldsymbol{x}) = h(x, y)$ denote the terrain function, which gives the terrain depth as a function of global horizontal position. We consider the following model for the measurements

$$\boldsymbol{\zeta}_k = \boldsymbol{h}_{\boldsymbol{\xi}_k, \boldsymbol{\eta}_k}(\boldsymbol{x}_k) + \boldsymbol{w}_k. \tag{2}$$

Here we have introduced the measurement vector function $\boldsymbol{h}_{\boldsymbol{\xi}_k, \boldsymbol{\eta}_k}(\boldsymbol{x}_k) = \{h_i\}_{i=1}^{m_k}$ with scalar components defined by

$$h_i = h(x_k + \xi_{k,i}^N, y_k + \eta_{k,i}^N) - \bar{h}_k - z_k + \bar{\zeta}_k, \tag{3}$$

and $\boldsymbol{w}_k$ is a white stochastic process modeling the bathymetric measurement error. This particular form of the measurement function is called *relative profile matching*, where the average of the measured profile $\bar{\zeta}_k$ (including vessel depth), and the corresponding average terrain profile $\bar{h}_k$, have been subtracted to eliminate potentially large unknown biases, e.g. due to tides. If $\bar{\zeta}_k = \bar{h}_k = 0$ the measurement function is called *absolute profile matching*.

Consider now a swath bathymeter, e.g. a multi beam echo sounder (MBE) or an interferometric sidescan sonar, where the measurement referenced in a local level vehicle body system B becomes $(\boldsymbol{0}, \boldsymbol{\eta}_k^B, \boldsymbol{\zeta}_k)$, assuming the measurements have been compensated for roll and pitch from the INS. If the vehicle moves directly forward, the measurements form a fan in the across track direction. The fan can be parameterized by a beam angle of the vertical, ϕ_i, and a one-way propagation time, τ_i, for the acoustic signal. The beam angle is estimated from angle of arrival estimation, and depends on sound speed as [8]

$$\frac{\partial \phi_i}{\partial c} = \frac{\tan(\phi_i)}{c}, \tag{4}$$

and τ_i is estimated from the bottom detection signal processing of the bathymeter. Here we only consider the case with constant sound speed throughout the water column. The vector of beam i from the body system to a point on the sea floor S, decomposed in N is then given by

$$\boldsymbol{p}_{BS,i}^N = \boldsymbol{R}_{NB} \begin{bmatrix} 0 \\ c\tau_i \sin\phi_i(c) \\ c\tau_i \cos\phi_i(c) \end{bmatrix}. \tag{5}$$

$\boldsymbol{R}_{NB} = \begin{bmatrix} \boldsymbol{e}_{B,x}^N & \boldsymbol{e}_{B,y}^N & \boldsymbol{e}_{B,z}^N \end{bmatrix}$ denotes the rotation matrix from B to N, a simple rotation about the vertical axis compensating for the vehicle's heading. By using the second and third unit column vectors of $\boldsymbol{R}_{NB}$ this can be written as

$$\boldsymbol{p}_{BS,i}^N = c\tau_i \left(\sin\phi_i(c) \boldsymbol{e}_{B,y}^N + \cos\phi_i(c) \boldsymbol{e}_{B,z}^N \right). \tag{6}$$

Finally, on component form the measurement depth of the acoustic bathymeter is given by

$$\zeta_{k,i} = \boldsymbol{p}_{BS,i}^N \cdot \boldsymbol{e}_{B,z}^N = c\tau_i \cos\phi_i(c), \tag{7}$$

and the horizontal footprint component is given by

$$\eta_{k,i} = \boldsymbol{p}_{BS,i}^N \cdot \boldsymbol{e}_{B,y}^N = c\tau_i \sin\phi_i(c). \tag{8}$$

The corresponding expected depth measurement from the terrain function is then given by

$$h_{k,i} = h(\boldsymbol{x}_k + \eta_{k,i} \boldsymbol{e}_{B,y}^N) - z_k. \tag{9}$$

C. Point mass filter estimator

The algorithm used in the HUGIN terrain navigation system [4] is based on the PMF, a nonlinear Bayesian estimator that estimates the probability density function (PDF) of the state vector on a grid [9], [10]. It was first used in aircraft terrain navigation [11], but has later made its way into underwater terrain navigation. Before introducing the actual PMF approximation, we consider the Bayesian formulation of the estimation problem (1) and (2).

We define a 2D bounded domain G_k in the earth tangent plane, enclosing the current INS solution. Let $\delta\boldsymbol{x}_k$ denote a position vector in G_k (the error of the INS) with reference to a north-aligned system with origin at the INS solution, and let Z_k denote the set of all measurements between t_1 and t_k. Our goal is to estimate the position error filter PDF $p(\delta\boldsymbol{x}_k | Z_k)$, conditioned on all the measurements so far in the *correlation period* $[t_0, t_k]$. From (1) we find that $\delta\boldsymbol{x}_k$ is a Markov process, and its PDF evolves in time according to the convolution integral [12]

$$p(\delta\boldsymbol{x}_{k+1} | Z_k) = \int_{G_k} p_{v_k}(\delta\boldsymbol{x}_{k+1} - \delta\boldsymbol{x}_k) p(\delta\boldsymbol{x}_k | Z_k) d\delta\boldsymbol{x}_k, \tag{10}$$

where $p_{v_k}(\cdot) = p(\delta\boldsymbol{x}_{k+1} | \delta\boldsymbol{x}_k)$ is the Markovian transition kernel for the error drift.

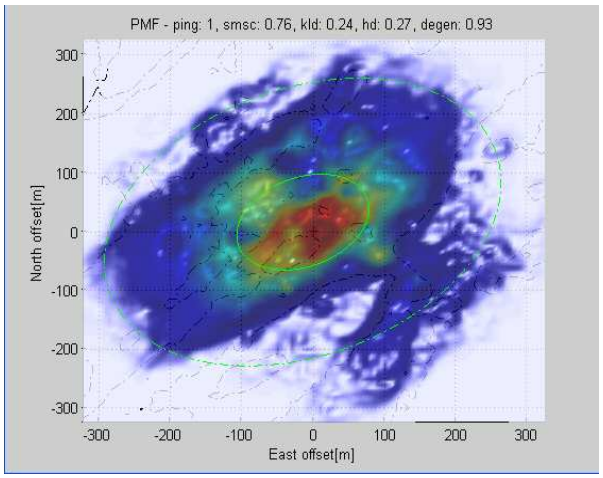

(a) Position error PDF after 1 ping

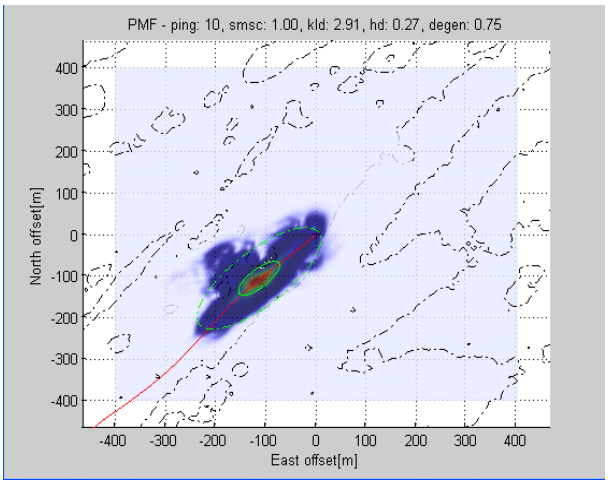

(b) Position error PDF after 10 pings

Fig. 2. Example of the position error PDF estimated by PMF after 1 (a) and 10 (b) pings, using only three beams from an EM710 multibeam echo sounder and 1 minute between each ping. True position is still recovered 100 m both south and west of the estimated position of the INS, which is always in the center of the 800 m x 800 m grid of the PMF.

The measurement update, following Bayes' theorem, is given by

$$p(\delta \boldsymbol{x}_k|Z_k) = \frac{p_{w_k}(\boldsymbol{\zeta}_k - \boldsymbol{h}_{\boldsymbol{\xi}_k,\boldsymbol{\eta}_k}(\boldsymbol{x}_k + \delta\boldsymbol{x}_k))p(\delta\boldsymbol{x}_k|Z_k)}{\alpha_k}, \tag{11}$$

where $\alpha_k = \int_{G_k} p_{w_k}(\boldsymbol{\zeta}_k - \boldsymbol{h}_{\boldsymbol{\xi}_k,\boldsymbol{\eta}_k}(\boldsymbol{x}_k + \delta\boldsymbol{x}_k))p(\delta\boldsymbol{x}_k|Z_k)d\delta\boldsymbol{x}_k$ is a normalization constant, and $p_{w_k}(\cdot)$ denotes the PDF for the sensor measurement error. Together the equations (10) and (11) form the recursive Bayesian estimator equations for terrain navigation. The recursion is started by a known initial PDF $p(\delta\boldsymbol{x}_0|Z_0) = p_0(\delta\boldsymbol{x}_0)$ at t_0 that depends on the initial INS accuracy, and the filter then runs recursively for each ping until a convergence or divergence criterion is met at t_K. The PMF approximation is found by representing the filter PDF in (10) and (11) by point masses on a regularly spaced grid representation of G_k, and by calculating the integrals through straightforward quadrature. Once the PMF approximation of the PDF is found, estimates of the INS position error and the accuracy of this estimate can be calculated directly from the approximated PDF [12]. Fig. 2 shows an example of the evolution of the PDF in the correlation period.

D. Tide and sound speed error model

To extend the PMF algorithm of terrain navigation to include concurrent modeling and estimation of tide and sound speed error, we will develop a first order linear model for the error. The Taylor series of the measurement (7) is given by

$$\zeta_{k,i} = \hat{\zeta}_{k,i} + \frac{\partial \zeta_{k,i}}{\partial c}\delta c + \frac{\partial \zeta_{k,i}}{\partial z_k}\delta z_k + ... \tag{12}$$

From (7) $\frac{\partial \zeta_{k,i}}{\partial z_k} = 0$ and

$$\frac{\partial \zeta_{k,i}}{\partial c} = \left(1 - \tan^2\phi_i\right)\frac{\zeta_{k,i}}{c} = \left(1 - \frac{\eta_{k,i}^2}{\zeta_{k,i}^2}\right)\frac{\zeta_{k,i}}{c}. \tag{13}$$

The corresponding Taylor series of the measurement model (9) is given by

$$h_{k,i} = \hat{h}_{k,i} + \frac{\partial h_{k,i}}{\partial c}\delta c + \frac{\partial h_{k,i}}{\partial z_k}\delta z_k + ... \tag{14}$$

From (9) $\frac{\partial h_{k,i}}{\partial z_k} = -1$ and

$$\frac{\partial h_{k,i}}{\partial c} = \nabla h \cdot \frac{\partial \eta_{k,i}}{\partial c}\boldsymbol{e}_{B,y}^N. \tag{15}$$

The footprint dependency on sound speed is found from (8)

$$\frac{\partial \eta_{k,i}}{\partial c} = \tau_i \sin\phi_i + c\tau_i \cos\phi_i \frac{\partial \phi_i}{\partial c} = 2\frac{\eta_{k,i}}{c}. \tag{16}$$

Finally, we can rewrite the measurement model equation (2) with a linear tide and sound speed error model given by

$$\hat{\boldsymbol{\zeta}}_k = \hat{\boldsymbol{h}}_{\boldsymbol{\xi}_k,\boldsymbol{\eta}_k}(\boldsymbol{x}_k) + \boldsymbol{H}_k\boldsymbol{\epsilon}_k + \boldsymbol{w}_k. \tag{17}$$

Here we have introduced the environment error state vector $\boldsymbol{\epsilon}_k = [\delta z, \delta c]_k^T$, and the $m_k \times 2$ matrix

$$H_{i,k} = \left[-1 \quad 2\frac{\eta_{i,k}}{c}\nabla h \cdot \boldsymbol{e}_{B,y}^N - \left(1 - \frac{\eta_{i,k}^2}{\zeta_{i,k}^2}\right)\frac{\zeta_{i,k}}{c}\right], \tag{18}$$

which projects the environment errors onto a corresponding depth error.

E. Modified PMF algorithms

The state of the estimation problem is now augmented by sound speed and depth errors, $[\delta\boldsymbol{x}, \boldsymbol{\epsilon}]$, making the problem four dimensional. The computational complexity of using a regular PMF directly on this problem is too high to be feasible for real-time applications [7], although a particle filter implementation could be considered [7], [13]. We instead consider three different modifications to the regular PMF.

1) PMF with General Least Square Estimate: Assume that the filter has converged to the true position $\boldsymbol{x}_k$. By defining the residual profile by $\boldsymbol{d}_k = \boldsymbol{\zeta}_k - \boldsymbol{h}_{\boldsymbol{\xi}_k,\boldsymbol{\eta}_k}(\boldsymbol{x}_k)$ the goal is to solve the estimation problem

$$\boldsymbol{d}_k = \boldsymbol{H}_k \boldsymbol{\epsilon}_k + \boldsymbol{w}_k. \tag{19}$$

We denote the measurement covariance matrix by $\boldsymbol{R}_k = E[\boldsymbol{w}_k \boldsymbol{w}_k^T]$, which now includes both the bathymetric sensor errors and the DTM errors. The analytic solution of the general linear least square (GLS) estimate is then given by [14]

$$\boldsymbol{\epsilon}_k = \left(\boldsymbol{H}_k^T \boldsymbol{R}_k^{-1} \boldsymbol{H}_k\right)^{-1} \boldsymbol{H}_k^T \boldsymbol{R}_k^{-1} \boldsymbol{d}_k \tag{20}$$

The estimate is unbiased and asymptotically normally distributed with covariance given by

$$\boldsymbol{P}_{\boldsymbol{\epsilon}_k} = E[\boldsymbol{\epsilon}_k \boldsymbol{\epsilon}_k^T] = \left(\boldsymbol{H}_k^T \boldsymbol{R}_k^{-1} \boldsymbol{H}_k\right)^{-1} \tag{21}$$

The modified version of the PMF is based on relative profile matching, and the GLS estimation of the sound speed and tide error is only done after the regular PMF has converged to an accurate position estimate. The estimated error are then compensated for subsequently in order to improve terrain navigation performance in less suitable terrain. These modifications to the algorithm is referred to as PMF-GLS.

2) PMF with sound speed and tide error model: This version is not really a modification of the regular relative profile matching PMF, but rather improves the error model by augmenting it with the tide and sound speed error model in (17), leading to a total error given by

$$\boldsymbol{w}_k' = \boldsymbol{H}_k \boldsymbol{\epsilon}_k + \boldsymbol{w}_k. \tag{22}$$

The term $\boldsymbol{w}_k$ only models DTM error and uncorrelated sensor errors. The modified covariance is then given by

$$\boldsymbol{R}_k' = \boldsymbol{H}_k \boldsymbol{P}_{\boldsymbol{\epsilon}_k} \boldsymbol{H}_k^T + \boldsymbol{R}_k. \tag{23}$$

This modified PMF algorithm is referred to as PMF-MOD.

F. Rao-Blackwellized PMF

Since the dynamic equation (constant tide and sound speed in the correlation period) and the measurement model is linear in the sound speed and depth error subspace containing $\boldsymbol{\epsilon}_k$, and the measurement and dynamic noise is modeled as Gaussian, the estimation problem can be solved by a Rao-Blackwellization of the PMF estimator. This technique has earlier been done in other estimation problems for particle filters [15]. By Bayes' theorem the joint PDF for the position and environmental errors is given by

$$p(\delta \boldsymbol{x}_k, \boldsymbol{\epsilon}_k | Z_k) = p(\delta \boldsymbol{x}_k | Z_k) p(\boldsymbol{\epsilon}_k | \delta \boldsymbol{x}_k, Z_k). \tag{24}$$

The first PDF factor is found using the PMF estimator in absolute profiling mode, and the second PDF factor can be optimally found using Kalman filters conditioned on each grid point of the PMF. Effectively, at each grid point of the 2D position error in the regular PMF, a Kalman filter is then maintained for the sound speed and depth error given the corresponding 2D position error. However, in cases of low gradient sea floors the first term in the second column of (18) can be ignored, and both the dynamic model and the linearized measurement model of the augmented subspace does not depend on the particular grid point. This means that a common Kalman gain $\boldsymbol{K}_k$, and covariance matrix $\boldsymbol{P}_{\boldsymbol{\epsilon}_k}$, is valid for the sound speed and tide error at each grid point. The analytical Kalman filter solution for grid point j is then given by [16]

$$\begin{aligned} \boldsymbol{\epsilon}_{k,j} &= \boldsymbol{\epsilon}_{k-1,j} + \boldsymbol{K}_k \left(\boldsymbol{\zeta}_k - \boldsymbol{h}_{\boldsymbol{\xi}_k,\boldsymbol{\eta}_k}(\boldsymbol{x}_k + \delta \boldsymbol{x}_{k,j}) - \boldsymbol{H}_k \boldsymbol{\epsilon}_k\right) \\ \boldsymbol{P}_{\boldsymbol{\epsilon}_k} &= \left(\boldsymbol{I} - \boldsymbol{K}_k \boldsymbol{H}_k\right) \boldsymbol{P}_{\boldsymbol{\epsilon}_{k-1}} \\ \boldsymbol{K}_k &= \boldsymbol{P}_{\boldsymbol{\epsilon}_{k-1}} \boldsymbol{H}_k^T \left(\boldsymbol{H}_k \boldsymbol{P}_{\boldsymbol{\epsilon}_{k-1}} \boldsymbol{H}_k^T + \boldsymbol{R}_k\right)^{-1}. \end{aligned} \tag{25}$$

This modified PMF algorithm is referred to as PMF-RB.

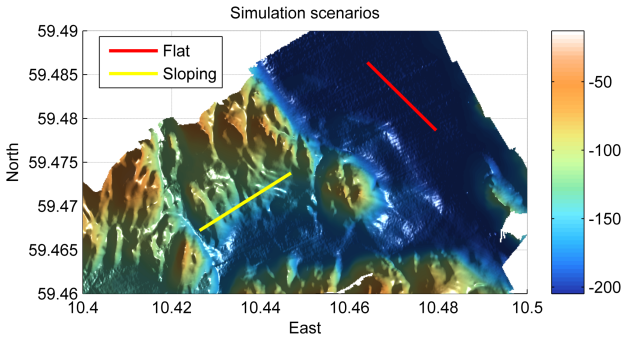

Fig. 3. Tracks for the two simulation scenarios overlaid the DTM: the flat terrain scenario (red), and the sloping terrain scenario (yellow).

III. Simulation Result

To get indications of performance of the algorithms, some simulations were performed and analyzed. The simulations consider a vessel traveling along at straight line at 2 m/s, carrying an MBE with a swath width of 130°. The algorithms use only 13 beams (uniformly spread in the swath width) from the MBE every third second.

The underlying terrain used in the simulations is based on a real DTM constructed from a survey outside Horten in the Oslo fjord. This DTM is considered as the true terrain, and another DTM was constructed based on adding white Gaussian noise with a standard deviation of 30 cm to the grid nodes of the true DTM. This simulated DTM was the one known to the algorithms.

The environmental errors were simulated by choosing a fixed 3 m tide level, while the algorithms initially assumed a nominal zero level. In addition a fixed 3 m/s of sound speed error was added to the nominal value of 1500 m/s, initially assumed by the algorithms. The measurement from the MBE was simulated by first computing a new unit beam vector based on the sound speed error and by using (4). The intersection between the new unit vector and the true DTM was then found, and used to calculate the range to the sea floor given this sound speed error. An additional white Gaussian error with standard deviation of 15 cm was finally added to the estimated range to the sea floor.

All the PMF algorithms were configured to use a 200 m

TABLE I
FLAT TERRAIN SCENARIO PERFORMANCE

Algorithm	Error	North [m]	East [m]	Depth [m]	Snd Spd [m/s]
PMF	Mean	-26.07	-27.89	-0.06	n/a
	Std Dev	25.21	68.75	0.12	n/a
PMF-MOD	Mean	0.25	-1.23	0.15	n/a
	Std Dev	2.93	2.67	0.07	n/a
PMF-GLS	Mean	1.64	0.10	-0.03	-0.01
	Std Dev	3.93	4.76	0.02	0.16
PMF-RB	Mean	1.39	0.08	-0.01	0.04
	Std Dev	2.26	1.81	0.02	0.08

TABLE II
SLOPING TERRAIN SCENARIO PERFORMANCE

Algorithm	Error	North [m]	East [m]	Depth [m]	Snd Spd [m/s]
PMF	Mean	-4.48	4.47	0.84	n/a
	Std Dev	4.36	4.93	0.33	n/a
PMF-MOD	Mean	-0.75	0.81	0.31	n/a
	Std Dev	1.59	2.06	0.19	n/a
PMF-GLS	Mean	-0.24	0.22	0.06	0.19
	Std Dev	2.01	2.61	0.33	0.65
PMF-RB	Mean	0.20	0.01	-0.01	0.03
	Std Dev	1.30	1.43	0.16	0.41

by 200 m grid with 1 m resolution. The initial PDF was chosen to be the uniform distribution, while the dynamic noise PDF was chosen to be a Gaussian with covariance based on 10 cm/s drift. Finally the measurement noise was modeled by a Gaussian combining the MBE noise and the DTM noise levels. The final covariance of the Gaussian used in the PMF estimator also includes the tide and sound speed error, as described for the different algorithms in Section II-E. The PMF algorithms all used the same set of convergence criterions for the approximated PDF. The criterions are based on a single modality measure, the similarity of the PDF to a Gaussian measured by the Hellinger distance, and the amount of information in the PDF measured by the Kullback-Leibler divergence [6].
Two scenarios were simulated. In the first scenario the vessel travels over flat parts of the terrain, and in the second over sloping parts of the terrain with some additional variations, see Fig. 3.

A. Flat terrain

This scenario lasts for 615 s, and the mean measured water depth is about 195 m. The terrain is mainly flat, but the swath with is about 800 m wide, so the MBE actually registers some variation in the outermost beam. The errors of the position and environmental states from all the algorithms are plotted in Fig. 4, and its mean and standard deviation are given in Table I. The regular PMF gets a few false position fixes, but diverges for most of the time. The false fixes are caused by the fact that the measurement noise occasionally correlates with the DTM noise in an otherwise flat terrain. In the HUGIN terrain navigation system [4] this would be detected and rejected by its integrity system. It is interesting and surprising that PMF-MOD is able to counter the false fixes and performs well simply through improved modeling, although not increasing the amount of position fixes to any degree. The PMF-GLS and PMF-RB algorithms get the highest amount of position fixes, which are all with highly accurate. They are also able to estimate both tide level and sound speed accurately in this scenario.

B. Sloping terrain

This scenario lasts for 687 s, and the mean measured water depth is about 140 m. The terrain is sloping with some additional variation to it. The swath width is about 600 m wide. The errors of the position and environmental states from all the algorithms are plotted in Fig. 5, and its mean and standard deviation are given in Table II. All the algorithms get a comparable amount of position fixes in this scenario. The PMF algorithm converges for all fixes but with a bias in the south-east direction, which coincides with the direction of the slope. This bias is caused by the fact that the algorithm is not able to estimate the tide level accurately enough. The PMF-MOD performs substantially better with only a corresponding bias of less than 1 m. The PMF-GLS and PMF-RB algorithms perform even better, and again they are able to estimate both the tide level and the sound speed accurately.

IV. CONCLUSION AND FUTURE WORK

Three different modifications to the regular PMF algorithm have been developed to enable concurrent estimation and compensation for tide and sound speed errors in terrain navigation. All three algorithms have been shown to perform well in simple simulation scenarios for flat and sloping terrain. Most surprisingly the simulations show a great performance increase in just improving the measurement model as in the PMF-MOD algorithm, but in both the scenarios the algorithms that concurrently also estimated both the tide and sound speed, the PMF-GLS and PMF-RB algorithms, performed better.
The simulations should be improved by including sound speed variations through the water column. And for improved assessment of the robustness and performance, Monte Carlo simulations of the scenarios should be done.
The real test is however performance on real data from both surface vessel and AUV.

REFERENCES

[1] J. Carlstrøm, "Results from sea trials of the Swedish AUV62F's terrain navigation system," in *15th International International Symposium on Unmanned Untethered Submersible Technology (UUST'07)*, Durham, NH, USA, 2007.

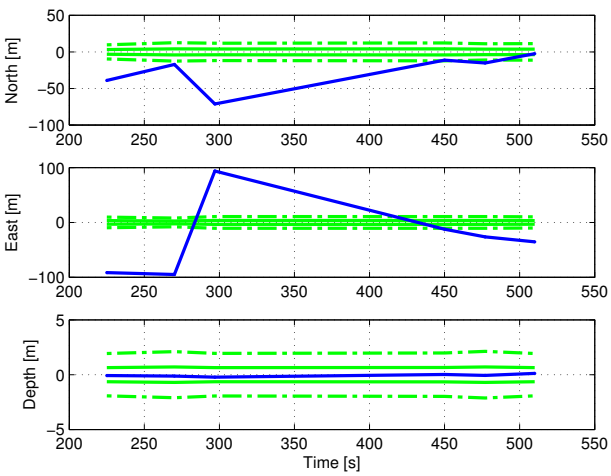

(a) PMF 6 position fixes

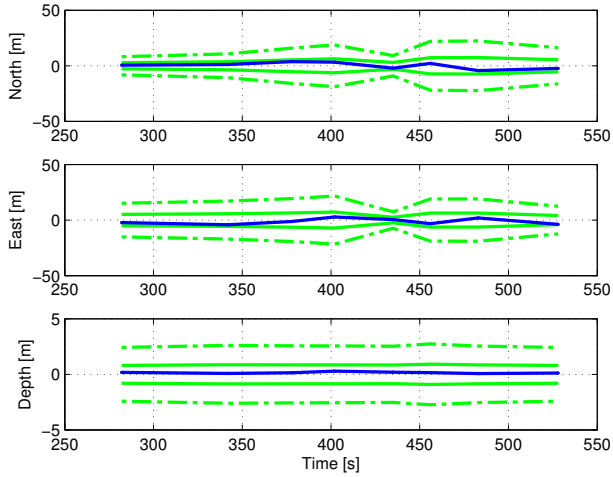

(b) PMF-MOD 8 position fixes

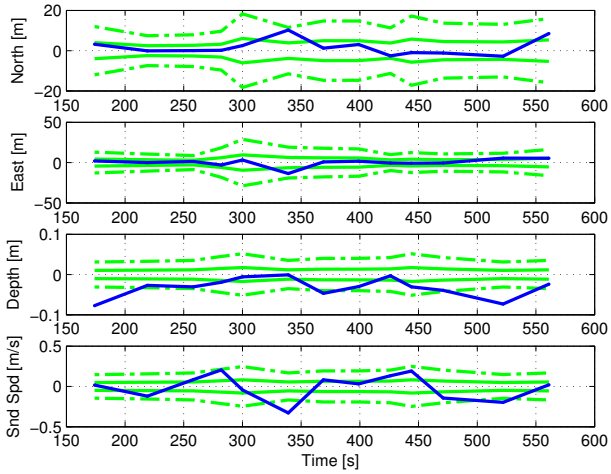

(c) PMF-GLS 13 position fixes

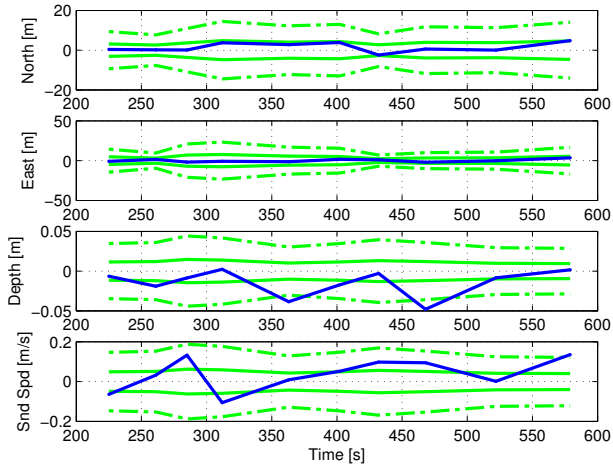

(d) PMF-RB 10 position fixes

Fig. 4. Flat terrain scenario performance for the regular PMF in (a), the PMF with added environmental modeling in (b), the PMF with decoupled linear least square environment estimation in (c) and the Rao-Blackwellized PMF in (d). The position and environment state errors (blue), along with estimated standard deviation 1σ (green) and 3σ (broken green).

[2] D. Meduna, S. Rock, and R. McEwen, "Closed-loop terrain relative navigation for auvs with non-inertial grade navigation sensors," in *2010 IEEE/OES Autonomous Underwater Vehicles (AUV)*, Monterey, CA , USA, 2010.

[3] G. Donovan, "Development and testing of a real-time terrain navigation method for auvs," in *OCEANS 2011*, 2011, pp. 1–9.

[4] O. K. Hagen, K. B. Ånonsen, and M. Mandt, "The HUGIN real-time terrain navigation system," in *Proceedings of the MTS/IEEE OCEANS 2010*, Seattle, WA, USA, 2010.

[5] O. K. Hagen, K. B. Ånonsen, and A. Skaugen, "Robust surface vessel navigation using terrain navigation," in *Proceedings of the MTS/IEEE Oceans Conference*, Bergen, Norway, June 2013.

[6] O. K. Hagen, K. B. Ånonsen, and T. O. Sæbø, "Low altitude AUV terrain navigation using an interferometric sidescan sonar," in *Proceedings of the MTS/IEEE OCEANS 2011*, Kona,HI,USA, 2011.

[7] K. Ånonsen and O. Hallingstad, "Terrain aided underwater navigation using point mass and particle filters," in *Proceedings of the IEEE/ION Position Location and Navigation Symposium (PLANS) 2006*, San Diego, CA, April 2006.

[8] D. Dinn, B. Loncarevic, and G. Costello, "The effect of sound velocity errors on multi-beam sonar depth accuracy," in *OCEANS '95. MTS/IEEE. Challenges of Our Changing Global Environment. Conference Proceedings.*, vol. 2, 1995, pp. 1001–1010 vol.2.

[9] R. Bucy, "Bayes theorem and digital realizations for non-linear filters," *The Journal of the Astronautical Sciences*, vol. XVII, no. 2, pp. 80–94, Sep.-Oct. 1969.

[10] R. Bucy and K. Senne, "Digital synthesis of non-linear filters," *Automatica*, vol. 7, no. 3, pp. 315–322, May 1971.

[11] N. Bergman, L. Ljung, and F. Gustafsson, "Terrain navigation using Bayesian statistics," *IEEE Control Systems Magazine*, vol. 19, no. 3, pp. 33–40, Jun. 1999.

[12] K. B. Ånonsen, "Advances in terrain aided navigation for underwater vehicles," Ph.D. dissertation, Norwegian University of Science and Technology, 2010.

[13] G. T. Donovan, "Position error correction for an autonomous underwater vehicle inertial navigation system (ins) using a particle filter," *IEEE Journal of Oceanic Engineering*, vol. 37, no. 3, pp. 431–445, 2012.

[14] A. Aitken, "On least squares and linear combination of observations," in *Proc. R. Soc. Edinb*, vol. 55, 1934, pp. 42–48.

[15] T. Schon, F. Gustafsson, and P. Nordlund, "Marginalized particle filters for mixed linear/nonlinear state-space models," *IEEE Transactions on Signal Processing*, vol. 53, no. 7, pp. 2279–2289, Jul. 2005.

[16] A. Gelb, Ed., *Applied Optimal Estimation*. Cambridge, MA: The MIT Press, 1974.

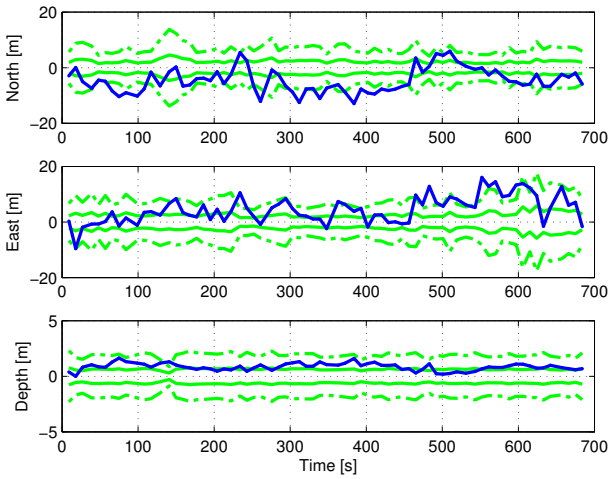

(a) PMF 71 position fixes

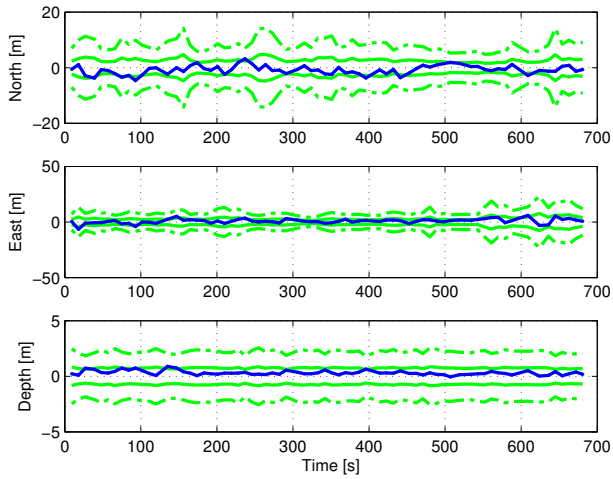

(b) PMF-MOD 69 position fixes

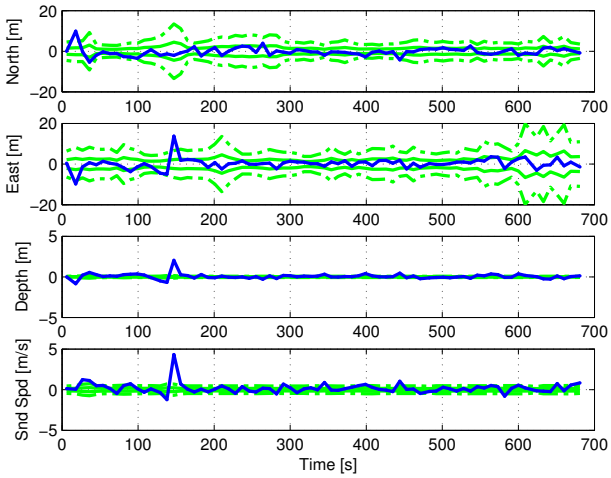

(c) PMF-GLS 74 position fixes

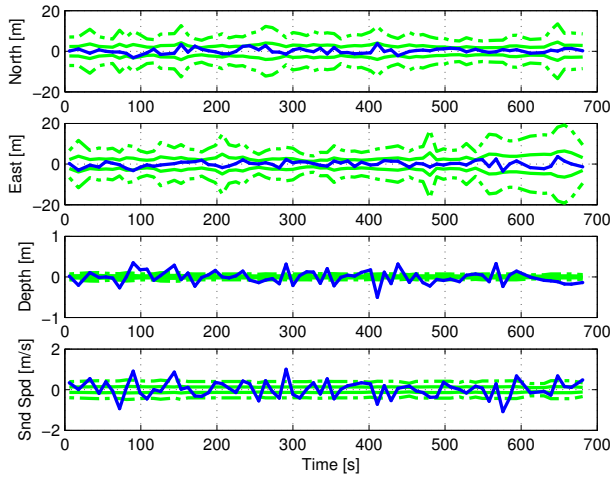

(d) PMF-RB 69 position fixes

Fig. 5. Sloping terrain scenario performance for the regular PMF in (a), the PMF with added environmental modeling in (b), the PMF with decoupled linear least square environment estimation in (c) and the Rao-Blackwellized PMF in (d). The position and environment state errors (blue), along with estimated standard deviation 1σ (green) and 3σ (broken green).